Supplementary Tables

		LeGUI				LeadDBS		
		x	y	z	d	x	y	z
Subject A	Left	-33.1	0.1	-4.2	0.40	-34.4	2.6	-4.1
Subject A	Right	32.4	6.0	-3.5	0.00	33.3	6.8	-5.0
Subject B	Left	-32.7	3.5	1.6	0.80	-34.0	1.4	0.1

Supplementary Table 1. Coordinates (x, y, z) in MNI space for claustrum microwires. Coordinates are displayed for localizations using both LeGUI and LeadDBS, respectively. Perpendicular axial distances (d, mm) in native space between claustrum microwires and the axial centerline of the claustrum are also shown.

		Claustrum				Anterior Cingulate				Amygdala			
		Left		Right		Left		Right		Left		Right	
		-	+	-	+	-	+	-	+	-	+	-	+
Subject A	Night 01	3	1	8	4	1	2	1	0	0	0	10	5
Subject B	Night 01	12	0			1	0	3	0	2	0	11	0
Subject B	Night 02	11	0			1	0	3	0	1	0	8	0
Subject B	Night 03	10	0			3	0	3	0	1	0	10	0

Supplementary Table 2. Number of single units per electrode and sleep recording. The "+" and "-" markers indicate positive- and negative-spiking units, respectively.

	Subject A Night 01	Subject B Night 01	Subject B Night 02	Subject B Night 03
W	40	181	154.5	165.5
R	8.5	122.5	128	104
N1	7	37.5	31.5	33.5
N2	62.5	234	303.5	305
N3	2	5.5	15	16

Supplementary Table 3. Sleep staging stratified by sleep recording (prior to artifact detection).

	Subject A		Subject B	
	Left	Right	Left	Right
Amygdala	1	2	3	2
Anterior insula	5	6	0	2
Hippocampus	1	1	1	2
Inferior frontal gyrus	1	4	0	5
Middle cingulate gyrus	1	0	0	0
Middle frontal gyrus	5	8	6	12
Middle temporal gyrus	2	6	2	4
Orbitofrontal gyrus	3	2	2	2
Posterior insula	4	0	0	0
Somatosensory	1	4	1	2
Superior frontal gyrus	3	0	0	0
Superior parietal lobule	3	2	0	4
Superior temporal gyrus	7	3	6	6
Premotor	0	1	0	3
Temporal pole	0	0	1	0
Inferior temporal gyrus	0	0	0	1
Motor	0	0	0	1
Fusiform gyrus	0	0	0	3
Posterior cingulate gyrus	0	0	0	2
Precuneus	0	0	0	1

Supplementary Table 4. Gray-matter macroelectrode contacts classified by customized regions of interest derived from the Yale Brain Atlas (prior to channel rejection).

MFG	Middle frontal gyrus
IFG	Inferior frontal gyrus
OFG	Orbitofrontal gyrus
PCC	Posterior cingulate cortex
PM	Premotor cortex
SPL	Superior parietal lobule
PNS	Precuneus
STG	Superior temporal gyrus
MTG	Middle temporal gyrus
TPL	Temporal pole
AMY	Amygdala
HPC	Hippocampus

Supplementary Table 5. Abbreviations for Figure 6g.

Supplementary Figures

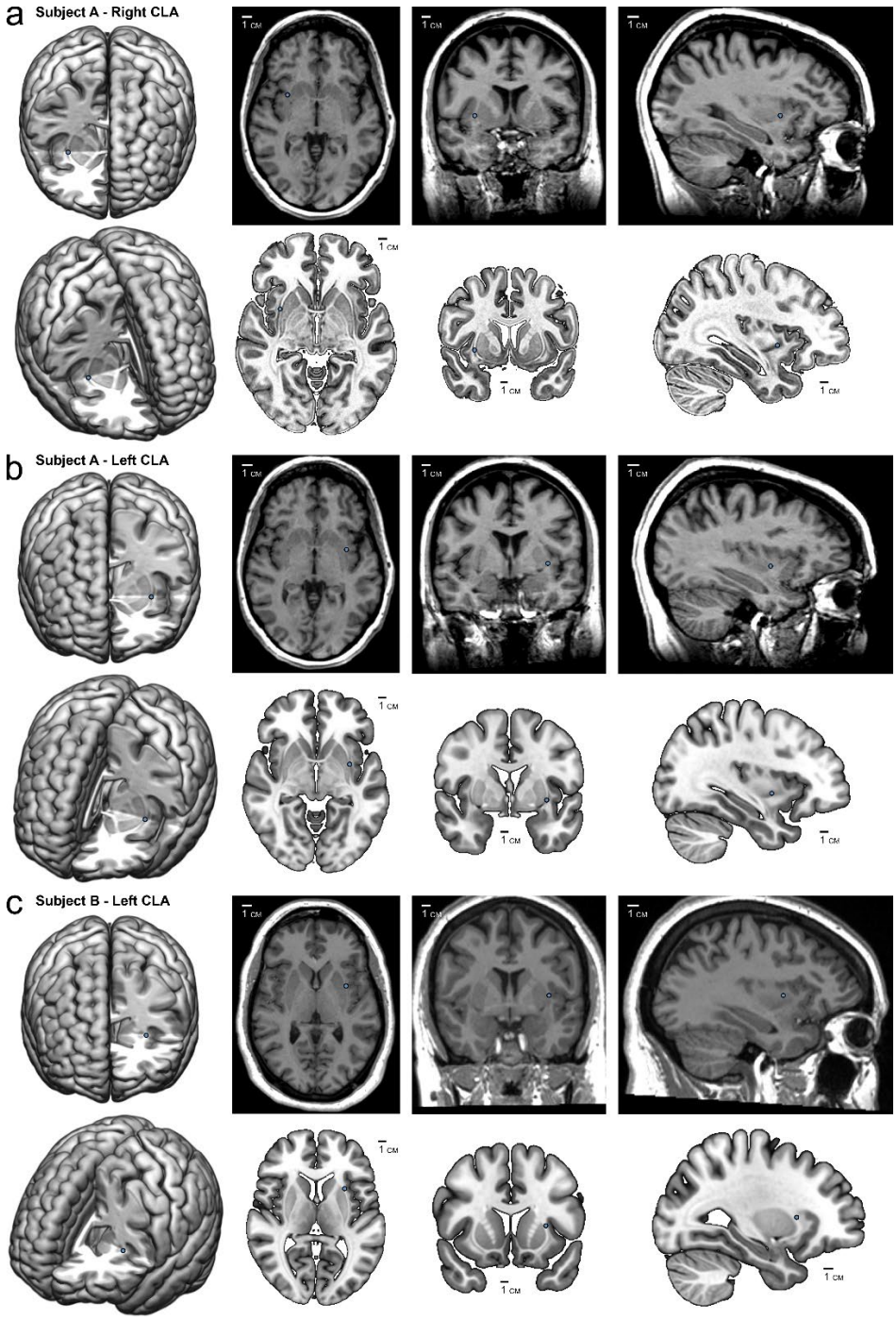

Supplementary Figure 1. Localization of claustrum microwires in LeGUI. (**a**) Subject A right claustrum, (**b**) Subject A left claustrum, and (**c**) Subject B left claustrum. Three-dimensional reconstructions on MNI152 brain models with cutouts to illustrate CLA microwire placement (blue dots) in anterior (top left) and oblique (bottom left) views. Placement is also demonstrated on T1 MRI axial (top left middle), coronal (top right middle), and sagittal (top right) slices of the subject MRI. The same views are shown in the bottom panels on the MNI152 template.

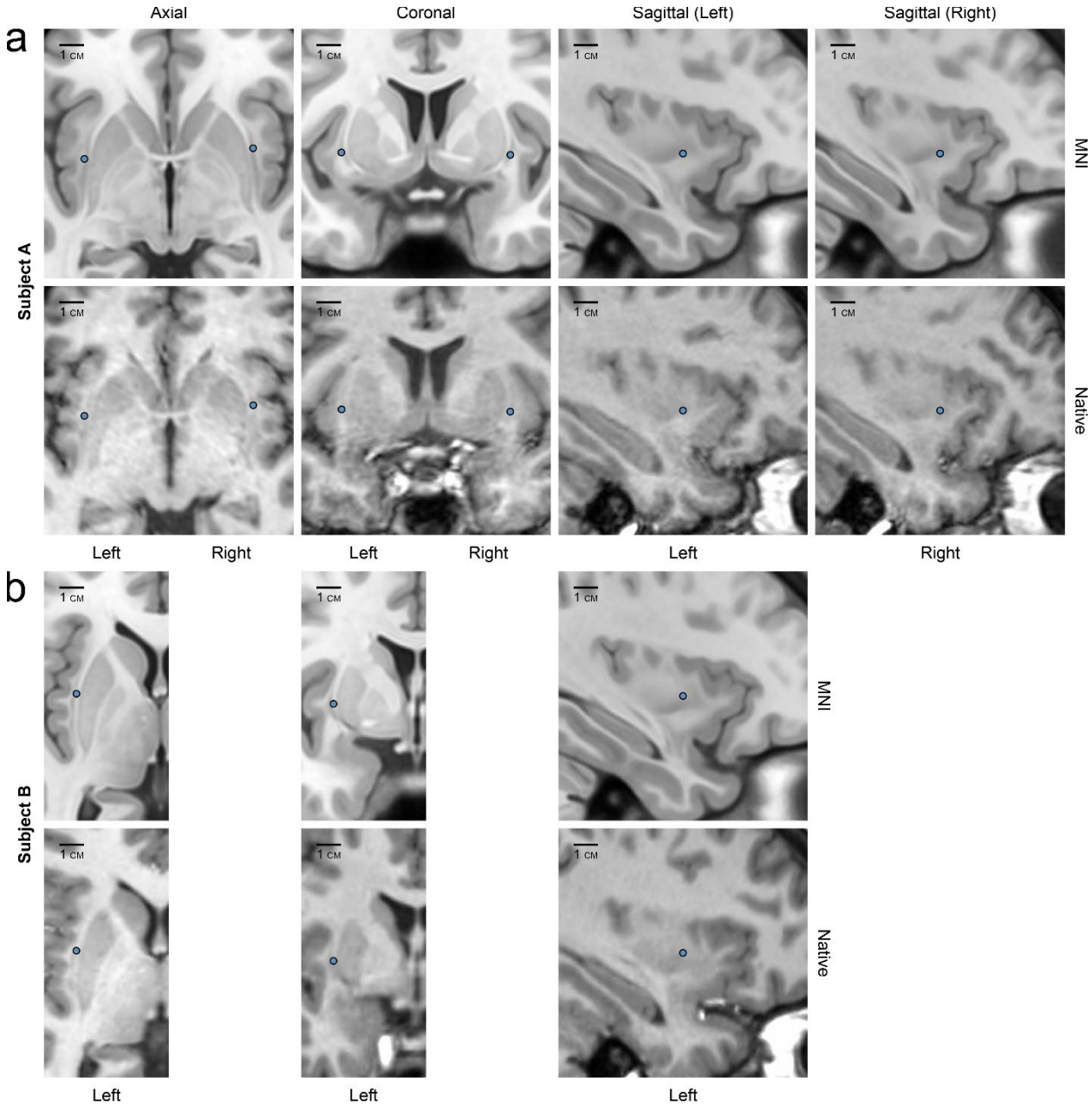

Supplementary Figure 2. Localization of claustrum microwires in LeadDBS. (a) Subject A bilateral claustrum (blue dots) in in axial (top left), coronal (top left middle), sagittal left (top right middle), and sagittal right (top right) views on the MNI152 template. The same views are shown in the bottom panels on the subject MRI. **(b)** Corresponding panels as in (a) are displayed with removal of right hemispheres given the unilateral claustrum microwire placement.

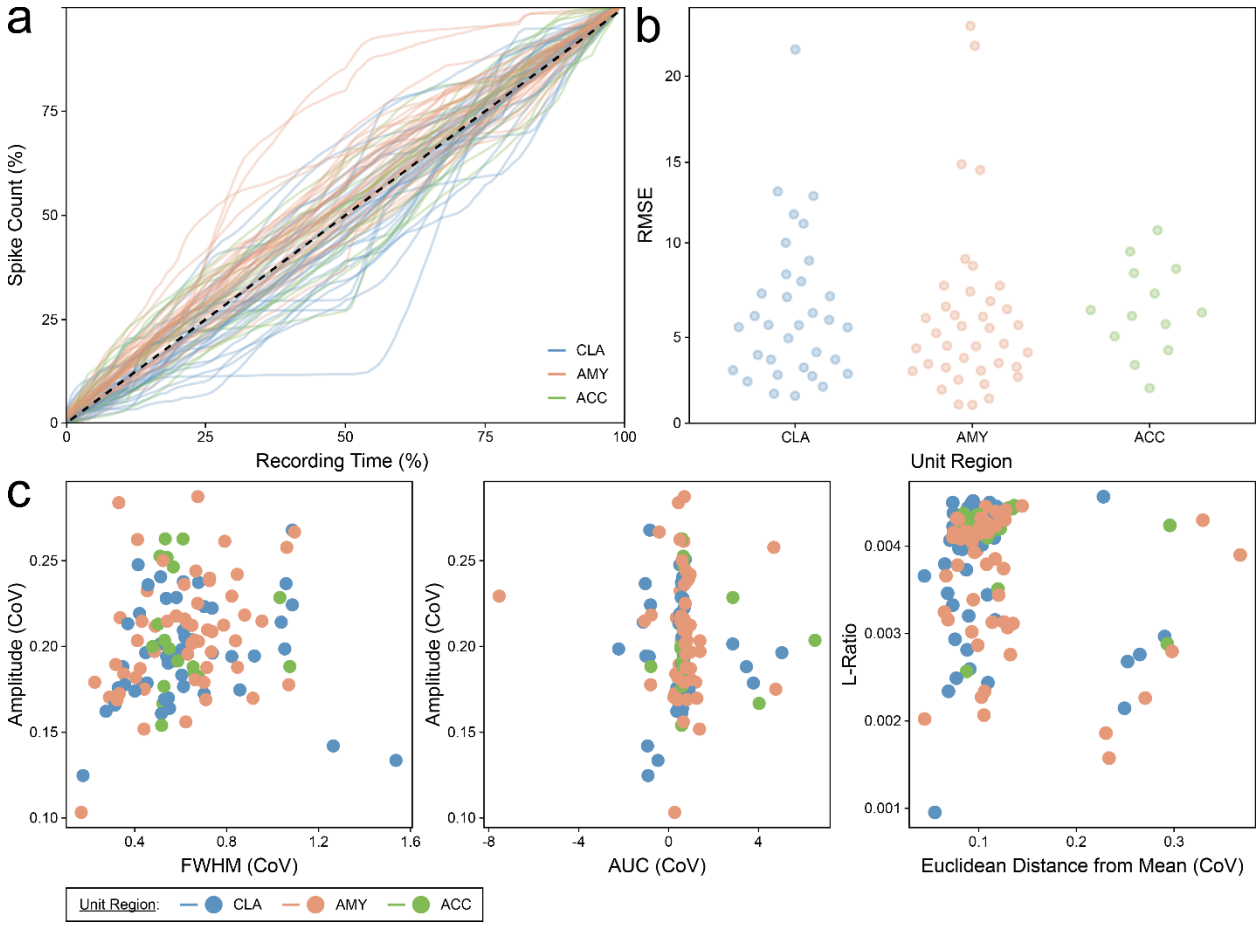

Supplementary Figure 3. Metrics of single unit stability. (a) Cumulative distribution of total detected spikes (%) across recording time (%) colored by unit region. **(b)** Dot plot of the root mean squared error (RMSE) of single unit cumulative distributions from the unity line stratified by unit region. **(c)** Scatterplots of waveform stability metrics for each single unit based on randomly sampled spikes. The coefficient of variation (CoV) is displayed for the waveform maximum amplitude, full width at half maximum (FWHM), area under the curve (AUC), Euclidean distance from mean. The L-ratio is also displayed. Colored by unit region.

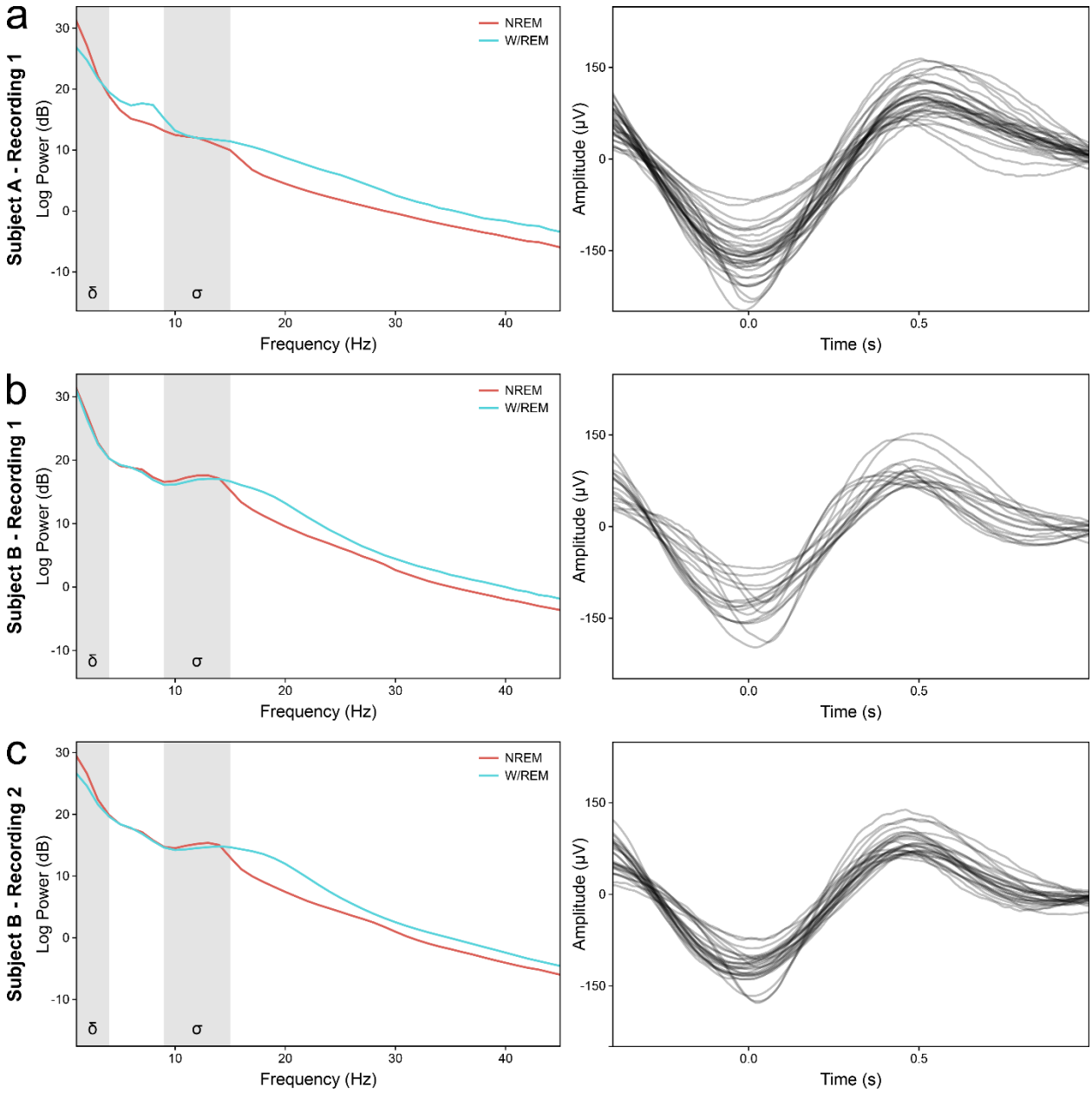

Supplementary Figure 4. Power spectral densities and slow-wave waveforms. (**a**) Subject A, Night 01, (**b**) Subject B, Night 01, and (**c**) Subject B, Night 02. Power spectral density plots of NREM (red) versus W/REM (blue) sleep across all macroelectrode channels (left panel). Delta and sigma frequency bands indicating SWA and sleep spindles, respectively (gray shading). Average waveforms of detected slow waves by macroelectrode channel (right).

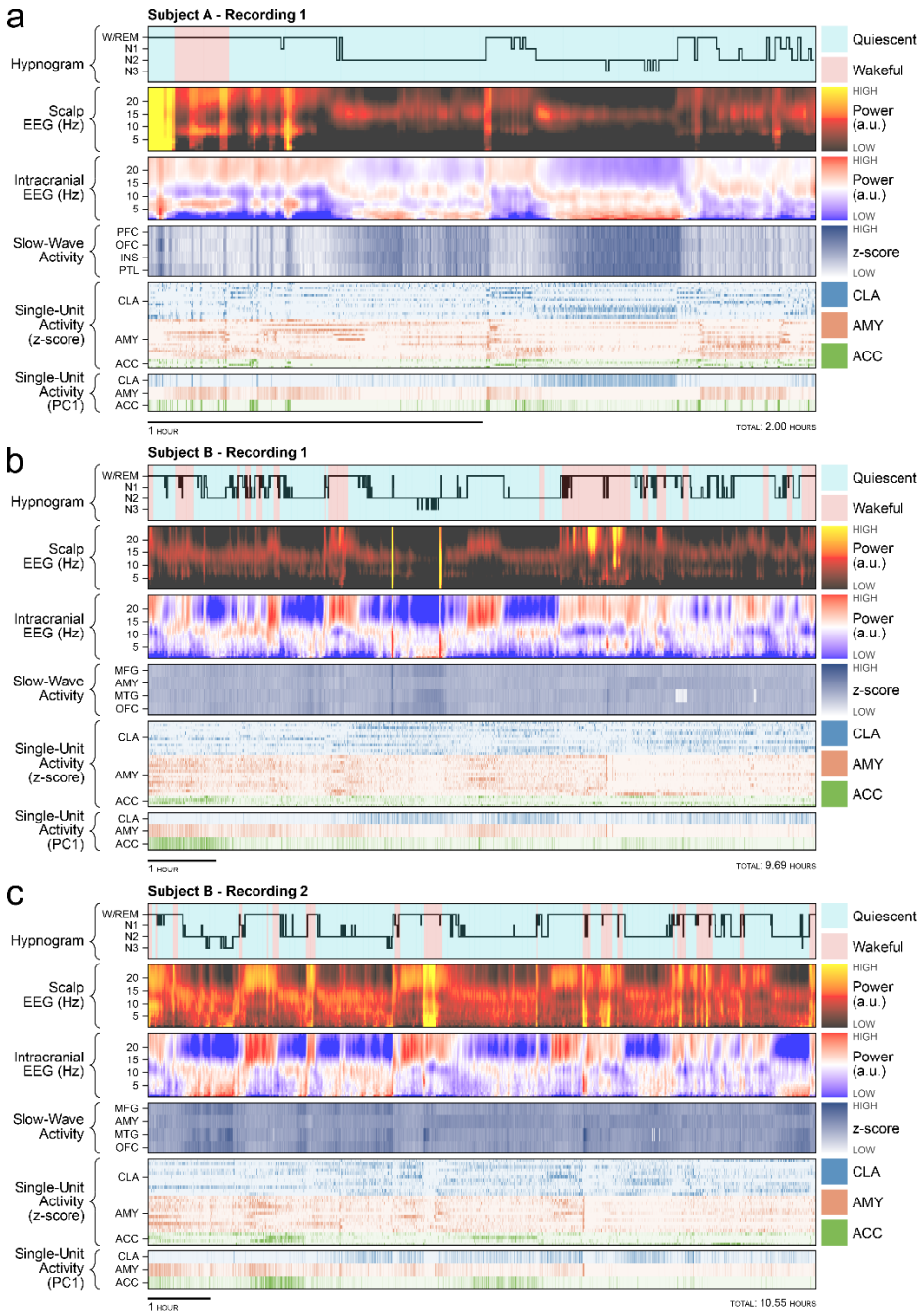

Supplementary Figure 5. Sleep recording overviews. (**a**) Subject A, Night 01, (**b**) Subject B, Night 01, and (**c**) Subject B, Night 02. Hypnogram shaded by behavioral state observed on avEEG: red indicates wakefulness and blue indicates behavioral quiescence (top row). Power spectrogram from the C4 scalp electrode (second row). Illustrative power spectrogram from the right middle frontal gyrus (third row). Binned z-score of slow-wave activity from four regions: middle frontal gyrus, amygdala, middle temporal gyrus, and orbitofrontal cortex (fourth row). Binned z-score of the firing rate for claustrum, anterior cingulate cortex, and amygdala single units; unit region indicated by colors (fifth row). First principal component of the firing rate in the single units of the same regions (sixth row).

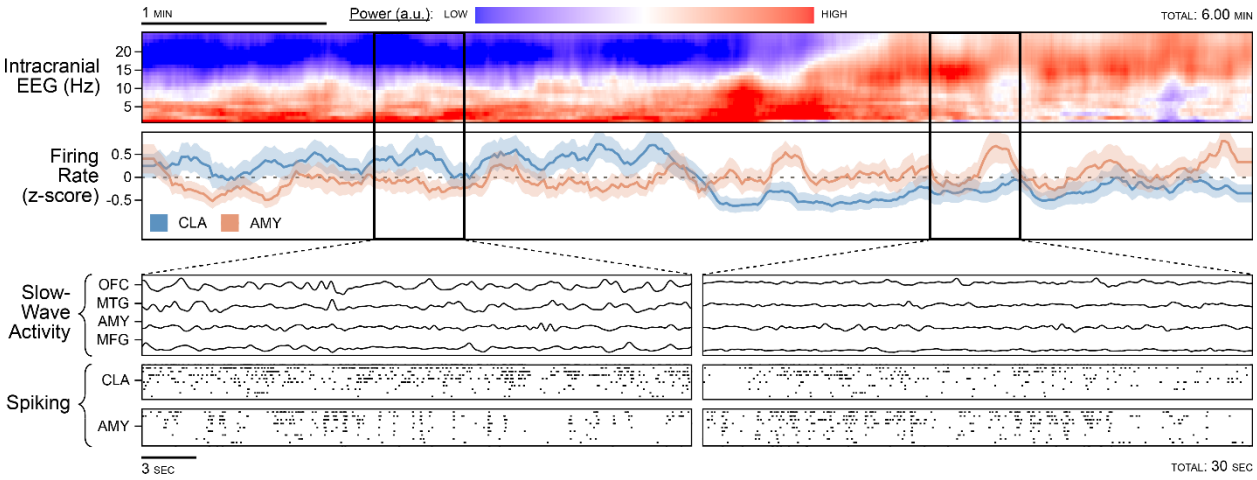

Supplementary Figure 6. Transition out of NREM sleep in Subject B, Night 02. Power spectrogram of left middle frontal macroelectrode centered on the time of sleep transition (first row). Z-score of population firing rates in the claustrum and amygdala; unit region indicated by colors (second row). Magnified time windows before and after the sleep transition (bottom left and bottom right panels, respectively) containing time series representations of slow-wave activity for intracranial macroelectrode channels in the orbitofrontal cortex, middle temporal gyrus, amygdala, and middle frontal gyrus (first rows of bottom panels) and single unit raster plots of spiking activity of the claustrum (second rows of bottom panels) and amygdala (third rows of bottom panels).

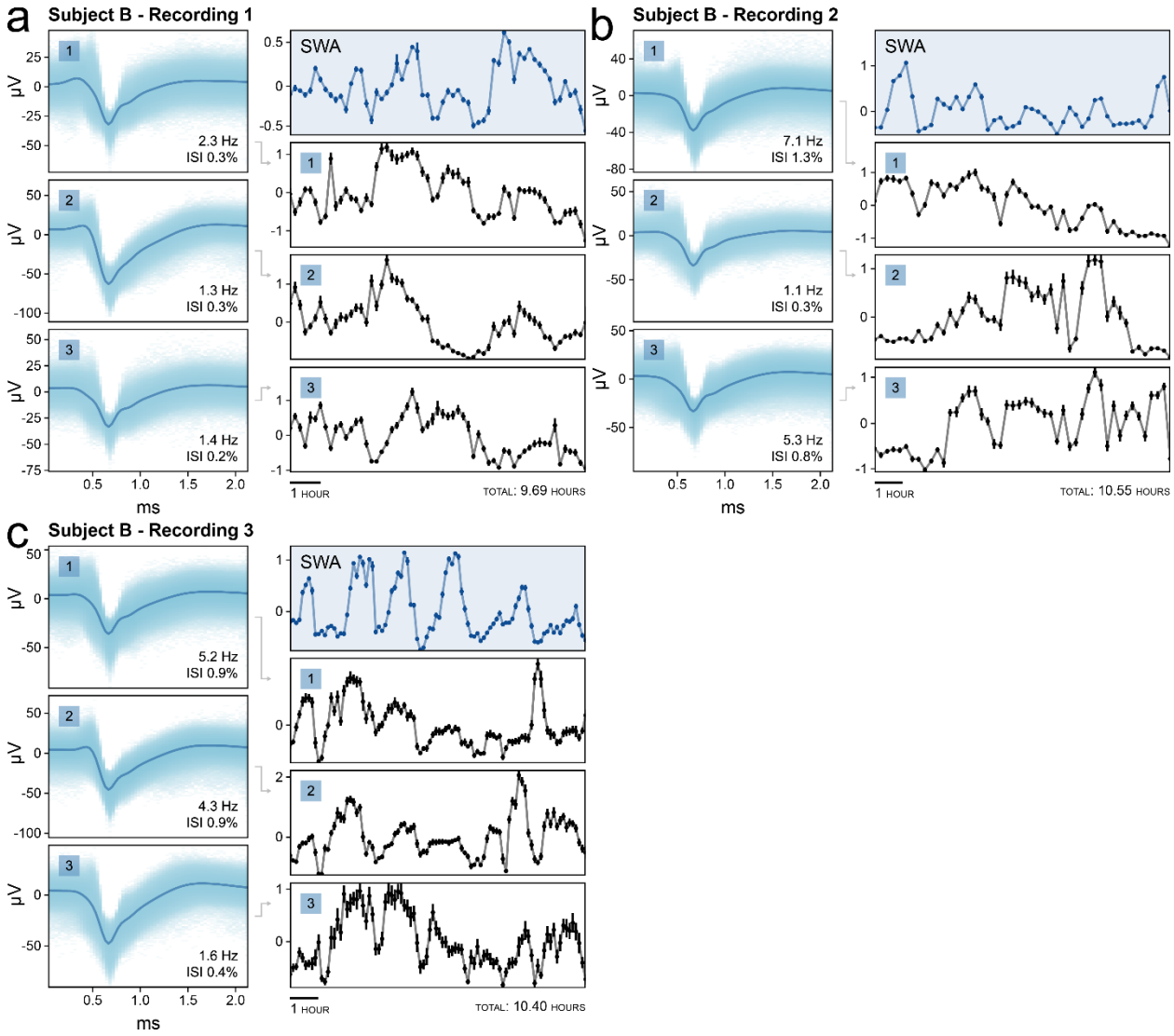

Supplementary Figure 7. Example claustrum single units tracking SWA and SWs. (**a**) Subject B, Night 01, (**b**) Subject B, Night 02, and (**c**) Subject B, Night 03. Average waveforms and inset unit statistics (firing rate, Hz, and inter-spike interval violations, %) of three example claustrum single units for each sleep recording (left panel). Corresponding binned time series of z-scored firing rates (black) of the units aligned with the binned z-scored time series of slow-wave activity (blue) in representative macroelectrode channels (right panel). Standard error for each 5-minute interval (30 epochs of 10 seconds each) is indicated by vertical bars.

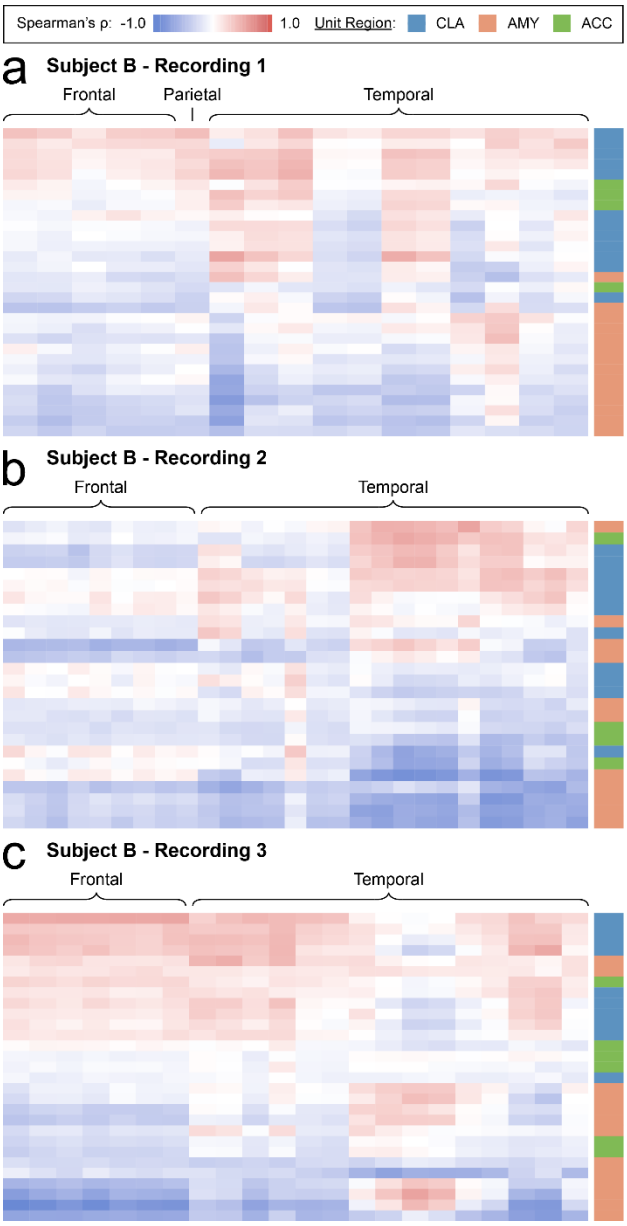

Supplementary Figure 8. Heatmap of Spearman's ρ correlations of unit-channel pairs. (**a**) Subject B, Night 01, (**b**) Subject B, Night 02, and (**c**) Subject B, Night 03. Single units are represented by rows and slow wave activity in macroelectrode channels are represented by columns. Unit region indicated by colors. Each cell is colored according to the strength of the Spearman's ρ correlation.

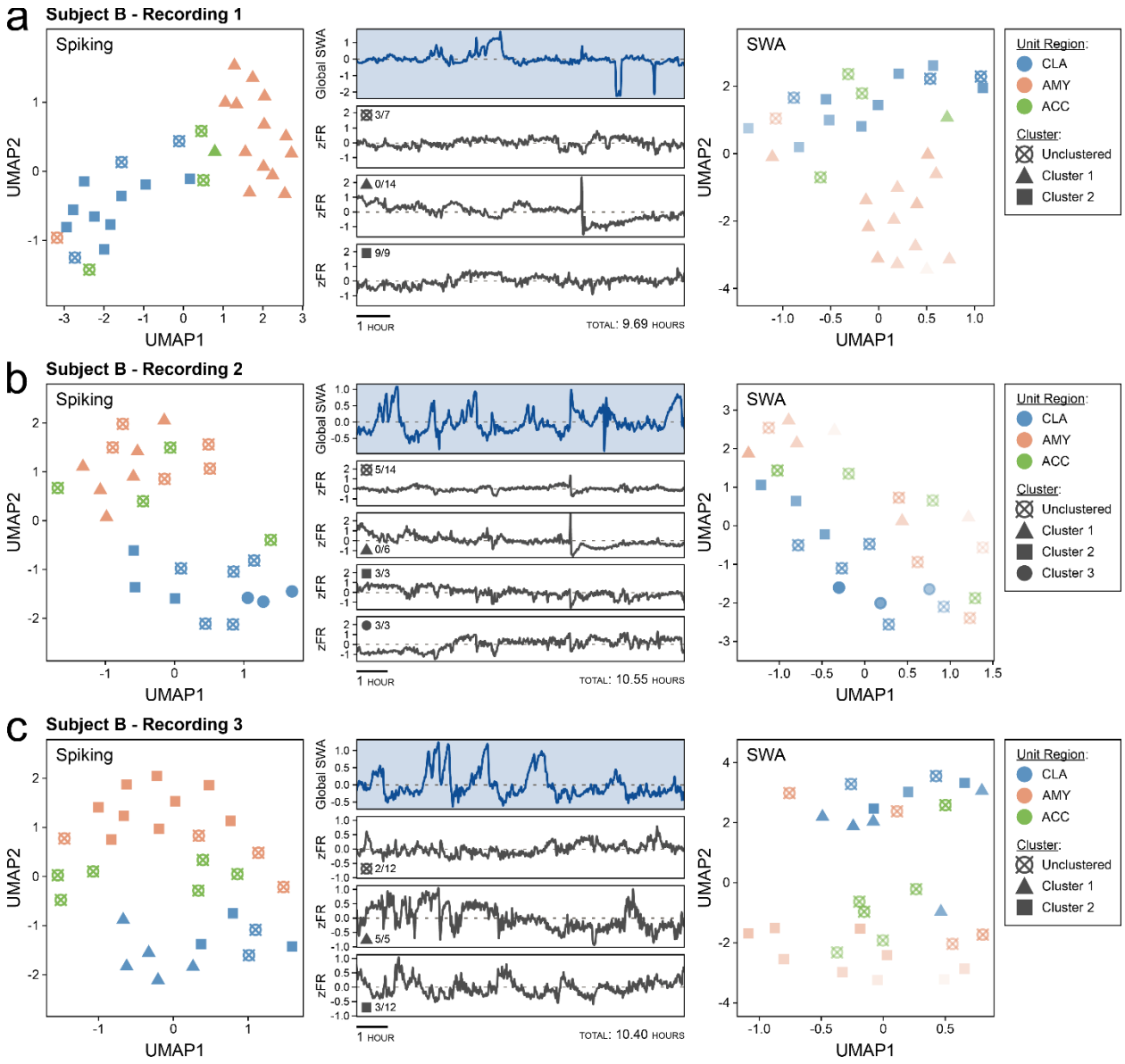

Supplementary Figure 9. Claustrum spiking and correlation separates from controls after dimensionality reduction. (**a**) Subject B, Night 01, (**b**) Subject B, Night 02, and (**c**) Subject B, Night 03. Scatterplot of two UMAP dimensions for single unit spiking activity demonstrates segregation of single units into HDBSCAN-defined clusters indicated by shapes; unclustered units are indicated by a crossed open circle; unit region indicated by colors (left panel). Time series of global slow-wave activity (middle panel, top row) with aligned time series representing z-scored population firing rates for clusters (middle panel, bottom rows). Scatterplot of two UMAP dimensions after dimensionality reduction of correlation with slow wave activity (right panel) across channels.